Effect and mechanism on the flotation desulfurization of high-sulfur bauxite by using the mixed collector of PYDH

Han Li [1], Qin Zhang [2,3,4]

[1] Mining College, Guizhou University, Guiyang 550025, China

[2] Guizhou Academy of Sciences, Guiyang 550001, China

[3] National & Local Joint Laboratory of Engineering for Effective Utilization of Regional Mineral Resources from Karst Areas, Guiyang 550025, China

[4] Guizhou Key Lab of Comprehensive Utilization of Nonmetallic Mineral Resources, Guiyang 550025, China

Corresponding author: zq6736@163.com (Qin Zhang)

Abstract: Desulfurization of high sulfur bauxite is an important issue in Bayer alumina production. In this study, by using two anionic sulphydryl collectors (HX, HD) as mixed collectors (PYDH), the selectivity of flotation separation between pyrite and diaspore was improved, thereby reducing the sulfur content of high sulfur bauxite and ultimately meeting the production requirements of Bayer alumina. The findings showed that under the optimized conditions of 500 g/Mg collector, 150 g/Mg inhibitor, 200 g/Mg activator, 100 g/Mg foaming agent, and a slurry pH of 9, the sulfur content of bauxite can be reduced from 3.35% to 0.33% through one rough selection, one fine selection, and one scavenging flotation. Moreover, the interaction mechanism between mixed collectors and pyrite was studied through scanning electron microscopy (SEM), Fourier transform infrared spectroscopy (FTIR), X-ray photoelectron spectroscopy (XPS), Zeta potential analysis, and contact angle testing. SEM-EDS research confirmed that PYDH adsorbed on the surface of pyrite. The contact angle measurement analysis showed that compared to individual collectors, pretreated pyrite with mixed collectors had better hydrophobicity. Zeta potential, FTIR, and XPS results indicated that PYDH selectively adsorbed pyrite through chemical adsorption. The mixed collector PYDH is an effective collector for pyrite in high sulfur bauxite flotation desulfurization.

Keywords: high-sulfur bauxite, flotation, mixed collector, desulfurization

1. Introduction

Aluminum has a wide range of applications and is the second most widely used metal after steel (Cheng et al., 2023). It finds wide applications in industries such as construction, transportation, power, and mechanical manufacturing. Bauxite is the main industrial raw material for alumina production. Aluminum hydroxide minerals in bauxite ore mainly composed gibbsite, boehmite and diaspore (Barbosa et al., 2016), there are different crystalline structure in these three minerals (Tabereaux et al., 2014). Diasporic bauxite has a significantly lower Al_2O_3 content and higher impurities than the gibbsitic bauxite. Bauxite deposits types include lateritic bauxites (mostly gibbsite and several traces of boehmite) and karst bauxites (typically diaspore), lateritic bauxites are bauxite deposits that occurred in laterite profiles directly overlie the original alumosilicate-rich lithotype and do exhibit a typical lateritic profile, Karst bauxite directly overlie a carbonate bedrock (Gibson et al., 2017; Mondillo et al., 2021). In China, bauxite is mainly of the diaspore type (Zhang et al., 2016), which is the main raw material for alumina production in China. With the utilization of bauxite resources, high-quality bauxite with a low content of resources is rapidly consumed, and there is an increasing attention on high sulfur bauxite (with sulfur content greater than 0.7%) (Paraskevas et al, 2016). High sulfur bauxite resources in China are distributed in Guizhou, Guangxi, Henan, Chongqing, Shandong and other provinces, with approximately 800 million tons of high sulfur bauxite (Zhou et al., 2019) not being fully utilized. However, excessive sulfur impurities in bauxite are one of the main obstacles in the Bayer process, for

example, reducing the quality of alumina products, increasing alkali consumption, decreasing heat conduction efficiency of evaporators, accelerating corrosion of equipment (Abikenova et al., 2008, Caldeira et al., 2003). Moreover, it also causes difficulties during washing of red mud (Liu et al., 2020). For this reason, desulfurization is necessary before high-sulfur bauxite used in alumina production, and desulfurization to eliminate its negative effects becomes a major challenge in alumina production.

More and more literature has studied the desulfurization of bauxite and adopted various methods, including wet desulfurization (Ge et al., 2015), pre roasting (Lou et al., 2016; Ersoy et al., 2013), microwave desulfurization (Li et al., 2015), potential controlled flotation (Yu et al., 2002; Awe et al., 2013), and biological desulfurization (Vera et al., 2013; Blight et al., 2000). However, due to their high cost and complex operation, these methods have not been widely applied in industrial production. Compared with other methods, flotation has the advantages of flexible operation and low cost, and has become a research hotspot for many scholars. Flotation (Bulut et al., 2004; Taguta et al., 2003) is currently an economically effective technology for desulfurization of high sulfur bauxite (Zhu et al, 2023).

Sulfur in high sulfur bauxite usually exists in the form of pyrite. Xanthate is the most commonly used pyrite collector in reverse flotation desulfurization of high sulfur bauxite (Yang et al., 2018; Xie et al., 2017). Sodium butyl xanthate has a wide range of applications in commercial scale industrial production among the xanthate. Dialkyl dithiophosphate, dithiocarbamates, thiols/thiophenols is also widely used collector for sulfide ore flotation (He et al, 2021; Liu et al, 2023; Chai et al, 2018). Besides, collectors such as hydroxamic acid, quaternary ammonium salt are also used in the sulfide ore flotation (Sun et al, 2021; Zhou et al, 2022). HX has good collection ability, while HD has similar collection performance to HX, but weaker collection ability and better selectivity, which can be used as mixed collector for desulfurization of high sulfur bauxite to obtain better flotation effect.

The mixed collector PYDH are used for reverse flotation desulfurization of high sulfur bauxite. The flotation conditions were optimized and closed-circuit tests were conducted. And its mechanism of action was studied. This study is expected to provide new references for the economic and efficient development and utilization of high sulfur bauxite.

2. Materials and methods

2.1. Materials

The bauxite ores used in these tests were collected from a certain area of China. The ores were crushed and ground until the particles were less than 2 mm and were mixed well.

The main chemical composition analysis results of raw ore are shown in Table 1.

Table 1 Element analysis results of high-sulfur bauxite sample

Elements	Al_2O_3	SiO_2	Fe_2O_3	TiO_2	K_2O	CaO	S
Content/%	60.97	11.54	6.46	3.10	1.78	0.90	3.35

The results of analysis indicate that the main chemical components of the ore sample are Al_2O_3, SiO_2, Fe_2O_3, TiO_2, and S. The content of Al_2O_3 is 60.97%, S is 3.35%, the A/S ratio is 5.28. Results show that this raw ore is typical low-grade bauxite with high-sulfur.

The mineralogical compositions are given in Fig. 1. As shown in Fig. 1, we found that it mainly consists of diaspore (valuable mineral), illite and sericite (gangue), pyrite (sulfur-contained mineral). As one of the main sulfur-contained minerals in bauxite, the removal of pyrite is of great significance to the desulfurization process of bauxite.

Main forms of sulfur in the ore should be determined first before desulfurization of high-sulfur bauxite, and then the corresponding desulfurization method should be selected. The analysis results of sulphur phase are shown in Table 2.

Table 2 Chemical phase analytic results of sulfur in high-sulfur bauxite

Phase	Element sulfur	Sulfide	Sulfate	Total
Content/%	0.01	2.96	0.38	3.35
Distribution rate/%	0.30	88.36	11.34	100.00

It can be seen in Table 2 that sulfide is the main existing form of sulfur, accounting for over 88%, followed by sulfate, the sulfur content in the form of elemental sulfur is relatively low. The sulfur in high-sulfur bauxite is mainly sulfide, containing a small amount of sulfate. It is difficult to remove sulfur sulfate through flotation, so the primary target mineral for desulfitization is pyrite.

As shown in Fig. 1, we found that it mainly consists of diaspore (valuable mineral), illite and sericite (gangue), pyrite (sulfur-contained mineral). As one of the main sulfur-contained minerals in bauxite, the removal of pyrite is of great significance to the desulfurization process of bauxite.

Main forms of sulfur in the ore should be determined first before desulfurization of high-sulfur bauxite, and then the corresponding desulfurization method should be selected. The analysis results of sulphur phase are shown in Table 2.
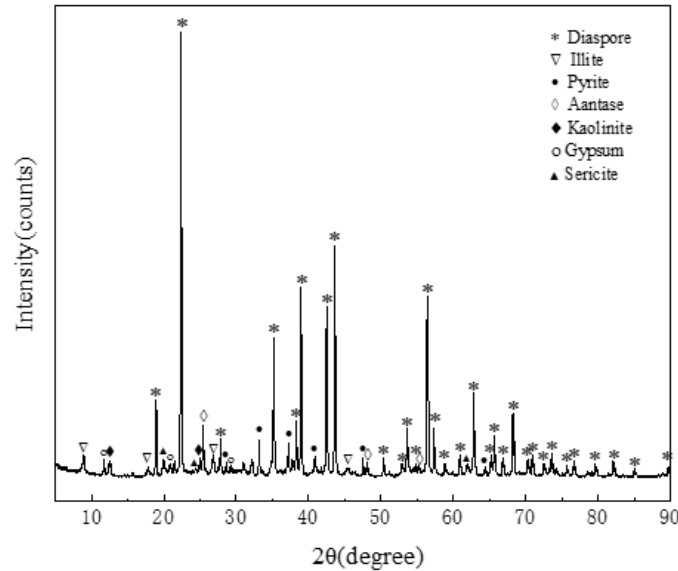

Fig. 1. XRD patterns of high-sulfur bauxite sample

Table 2 Chemical phase analytic results of sulfur in high-sulfur bauxite

Phase	Element sulfur	Sulfide	Sulfate	Total
Content/%	0.01	2.96	0.38	3.35
Distribution rate/%	0.30	88.36	11.34	100.00

It can be seen in Table 2 that sulfide is the main existing form of sulfur, accounting for over 88%, followed by sulfate, the sulfur content in the form of elemental sulfur is relatively low. The sulfur in high-sulfur bauxite is mainly sulfide, containing a small amount of sulfate. It is difficult to remove sulfur sulfate through flotation, so the primary target mineral for desulfitization is pyrite.

2.2. Methods

2.2.1. Flotation test

All flotation experiments were performed in a flotation cell (1.5 L, XRF, China), and the agitation speed was 2000 rpm. The 500 g crushed mineral sample was ground by a ball mill before flotation. The concentrates (in-tank product) and tailings (froth product) were collected, filtered, then dried and weighted after flotation. The flotation tests were conducted in accordance with the flow sheet shown in Fig. 2, the yield and recovery were calculated based on the weight distribution of mineral particles between concentrates and tailings, these can be calculated as follows:

$$Yield(\gamma) = \frac{q}{Q} \tag{1}$$

$$Recovery(\varepsilon) = \frac{\gamma\beta}{\alpha} \tag{2}$$

$$Desulfurization\ degree(R) = \frac{\alpha - \gamma_1\beta}{\alpha} \tag{3}$$

where q is the weight of flotation products and Q is the weight of raw ore, α and β respectively represents the grade of raw ore and concentrate, γ_1 is the yield of the concentrate.
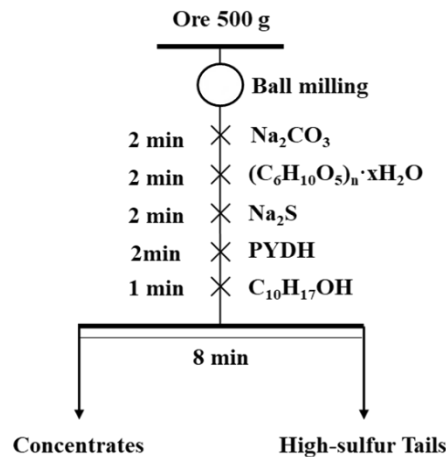

Fig. 2. Schematic diagram of the desulfurization flotation of high-sulfur bauxite

2.2.2. Characterization method

X-ray diffraction (XRD) of the sample was run on the D8 Advance (Bruker, DE) with Cu Kα radiation. The samples were scanned at a scan rate of 2 min^{-1} in a 2θ ranges of 5°–90°.

The observation of mineral morphology characteristics was completed by scanning electron microscope (SEM). The sample was in powder form and was first treated with gold spraying at 10 mA. The scanning electron microscope model used was GeminiSEM 300 (ZEISS, DE), the energy spectrometer model was OXFORD Xplore. The acceleration voltage during topography shooting was 3 kV, and the acceleration voltage during energy spectrum mapping shooting was 15 kV. The detector was SE2 secondary electron detector. The working distance is adjusted according to the actual situation.

The contact angles of pyrite before and after adding collectors were measured using a sessile drop method by a JY-82B Kruss DSA Contact angle tester (Shimadzu, Japan). The contact angle was measured by pressing pyrite particles of -38 μm into pellets with a diameter of 2 cm. By taking measurements at different points in the same pellet three times, the average contact angle value was determined.

Zeta potential of pyrite before and after adding collectors was collected using DelsaTM Nano C Zeta potential analyzer (Beckman, US). A suspension containing 0.05 wt% mineral particles, which was ground to -25 μm, was prepared in KCl solution with a concentration of 10^{-3} mol/L. After settling for 24 h, take 10 cm^3 of suspension for adding reagents and adjust the pH value. Then stir for 10 min until the particles were completely distributed. Add it to the sample cell for Zeta potential measurement after settling for 20 min. This step was repeated three times to take the average value.

X-ray photoelectron spectroscopy (XPS) analysis was carried out using a K-alpha (Thermo, USA), using a pass energy of 187.85 eV with a step size of 0.8 eV.

Infrared spectra of pyrite interacted with and without collectors were carried out using Nicolet IS5 (Thermo, USA). Approximately 1 mg sample was placed in 100 mg of spectroscopic-grade KBr to mix well and pressed into the pellet for recording the spectrum.

2.3. Reagents

The reagents used in this work included sodium carbonate (pH regulator, ≥95%, purity), amylopectin from maize (inhibitor, ≥95%, purity), cupric sulphate and sodium sulfide nonahydrate (activator, ≥95%, purity), PYDH (collector, ≥90%, purity) and terpenic oil (foaming agent, natural, purity). PYDH used as collectors, sodium carbonate used as pH regulator, amylopectin used as inhibitor, and cupric sulphate and sodium sulfide nonahydrate used as activator, these was prepared into an aqueous solution with a mass percentage concentration of 1%. Sodium carbonate used as pH regulator, it was prepared into an aqueous solution with a mass percentage concentration of 5%. All the reagents were ready-to-use to avoid drug failure. Sodium carbonate, amylopectin, cupric sulphate and sodium sulfide nonahydrate

were obtained from Aladdin Industrial Corporation, China, PYDH was supplied by Maya Reagent, China, terpenic oil was bought from Tianjin Kermel Reagent Technologies Co., Ltd., China.

3.   Results and discussion

3.1.   Flotation tests

3.1.1.   Influence of flotation condition on desulfurization

A series of flotation tests were conducted under the conditions of a pulp pH of 9, PYDH dosage of 400 g/Mg, the amylopectin dosage of 150 g/Mg, sodium sulfide nonahydrate dosage of 200 g/Mg, terpenic oil dosage of 100 g/Mg to obtain good grinding fineness. Fig. 3 presents the date on effect of particle size, with the increase of grinding fineness, the sulfur content of concentrate gradually decreased, and the desulfurization degree showed an increasing trend. Taking the energy consumption of grinding into account, −0.075 mm is appropriate grinding fineness, accounting for 79.55% with a lower sulfur content of the concentrate. Grinding fineness was determined to be −0.075 mm, 79.55%.

The second set of experiments, as illustrated in Fig. 4, was designed to investigate the impact of pulp pH. With the increase of pulp pH, the sulfur content of concentrate gradually decreased and desulfurization degree increased. Moreover, the concentrate contained lower contents of sulfur at pH 9-10, in the range of 0.37%-0.39%, and the values of desulfurization degree are very close to each other, within a range of 89.40–90.14%. Selecting 9 as pulp pH in order to reduce alkali consumption.
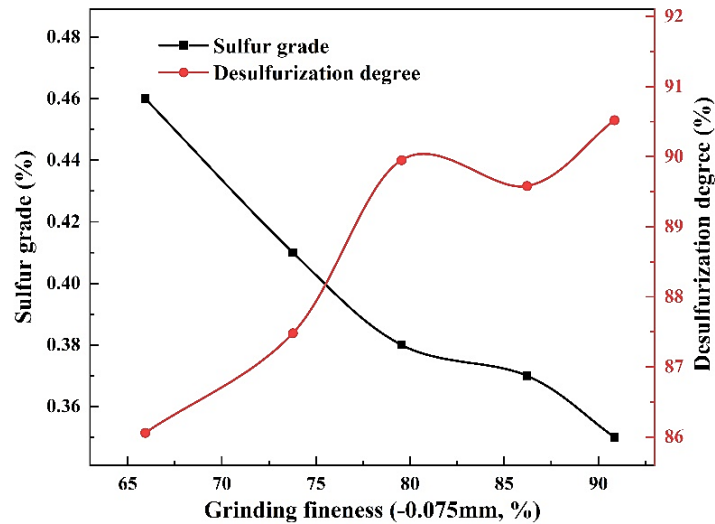

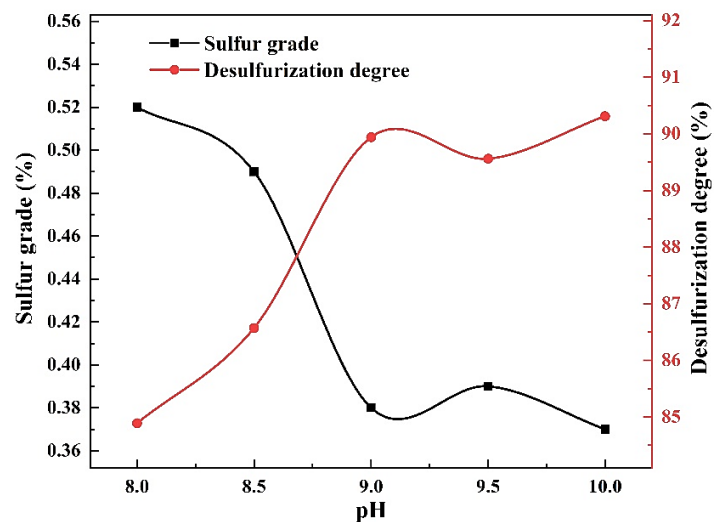Fig. 3. Effects of grinding fineness on desulfurization

Fig. 4. Effects of pulp pH on desulfurization

The effect of PYDH dosage on desulfurization is shown in Figure 5. The sulfur content of the concentrate shows a trend of first decreasing and then increasing, as the amount of PYDH increases, the desulfurization rate shows a trend of first increasing and then decreasing. When PYDH dosage is 500 g/Mg, the sulfur content reaches the minimum value and the desulfurization degree reaches the maximum value. In summary, the appropriate amount of PYDH is 500 g/Mg.

The results on effects of inhibitor dosage are presented in Fig. 6. We see sulfur content of concentrate first falls with increase of inhibitor dosage and then rise, however desulfurization degree firstly increases and then decrease as the inhibitor dosage grows. There is lower sulfur content (0.38%-0.40%) and desulfurization degree (88.17%-88.52%) at an inhibitor dosage of 150 g/Mg and 200 g/Mg, so, the inhibitor dosage of 150 g/Mg was appropriate when considering reagents costs.
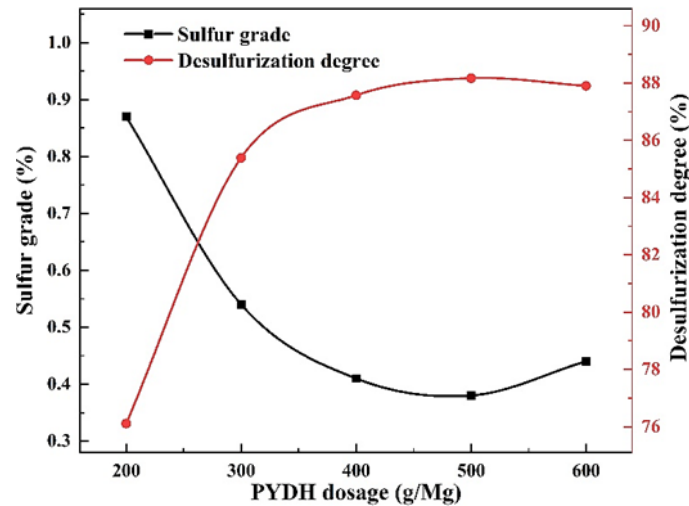

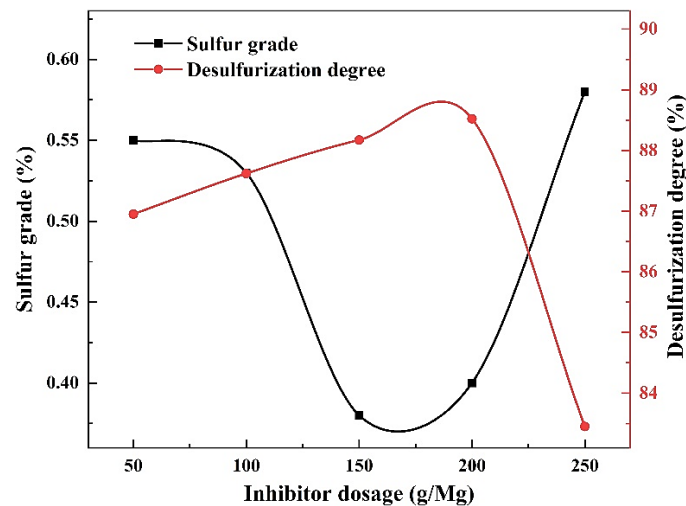
Fig. 5. Effects of PYDH dosage on desulfurization

Fig. 6. Effects of inhibitor dosage on desulfurization

A series of flotations were tested under the conditions of different dosage ratio of $CuSO_4$/ Na_2S (1:1, 1:2, 1:4, 2:1, 4:1). And we also used cupric sulphate or sodium sulfide nonahydrate as activator alone for comparison in this experiment. Table 3 presents the data provided by the experiments on effects of ratio of activator on desulfurization. It is apparent from this table that the best results for desulfurization have been achieved when dosage ratio of $CuSO_4$/ Na_2S is 4:1. The sulfur content of concentrate is 0.32% and the desulfurization degree is 91.33%. We, therefore, chose 4:1 for the dosage ratio of $CuSO_4$/ Na_2S as activator.

From the data in Figure 7, it is apparent that the sulfur content of concentrate decreased to the minimum (0.32%) and the desulfurization degree increased to the maximum (91.33%) at activator

dosage of 200 g/Mg. As a result, based on the change trends, the amount of activator used in the subsequent experiments is 200 g/Mg.

Table 3 Effects of ratio of activator on desulfurization

| collector composition	Product	Yield/wt %	$\omega(S)/\%$	desulfurization degree/%
CuSO$_4$	concentrate	83.70	0.36	90.17
	tailing	16.30	16.96	
Na$_2$S	concentrate	80.97	0.37	90.24
	tailing	19.03	14.55	
CuSO$_4$/ Na$_2$S =1:1	concentrate	81.43	0.37	89.53
	tailing	18.57	13.87	
CuSO$_4$/ Na$_2$S =2:1	concentrate	81.09	0.33	90.98
	tailing	18.91	14.28	
CuSO$_4$/ Na$_2$S =4:1	concentrate	82.49	0.32	91.33
	tailing	17.51	15.89	
CuSO$_4$/ Na$_2$S =1:2	concentrate	81.44	0.34	90.70
	tailing	18.56	14.55	
CuSO$_4$/ Na$_2$S =1:4	concentrate	80.70	0.38	89.05
	tailing	19.30	12.92	
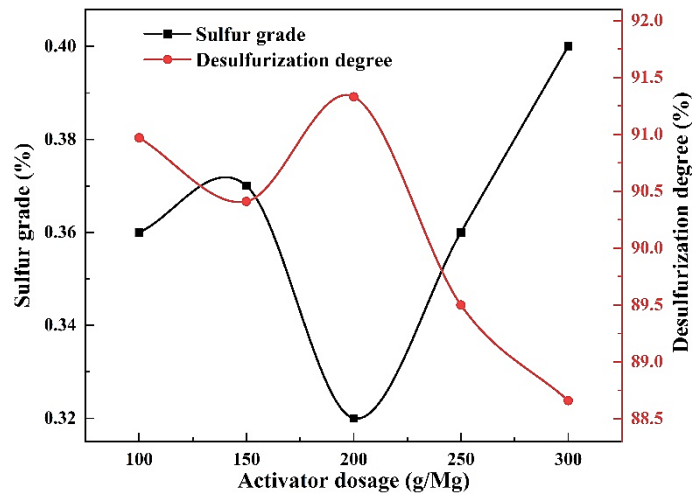
Fig. 7. Effects of activator dosage on desulfurization

Fig. 8 shows the results obtained from the studies of effects of foaming agent dosage on desulfurization. The value of sulfur content of concentrate first goes down and then goes up with increase of foaming agent dosage. On the contrary, with the increase of foaming agent dosage, the desulfurization rate significantly increases and then decreases. When the dosage of foaming agent is 100 g/Mg, the sulfur content reaches the minimum value and the desulfurization degree reaches the maximum value, indicating that the appropriate dosage of foaming agent is 100 g/Mg.

The results of flotation test provide optimum reverse flotation conditions of high-sulfur bauxite. Finally, the most suitable regime of agent in the roughing stage is: grinding fineness of -0.075 mm, 79.55%, slurry pH of 9, PYDH dosage of 500 g/Mg, branched starch dosage of 150 g/Mg, CuSO$_4$/Na$_2$S (4:1) dosage of 200 g/Mg, and terpenic oil dosage of 100 g/Mg. Based on the above series of conditions, an opened-circuit test of one roughing, one cleaning and one scavenging was conducted. The sulfur content of concentrate could be reduced to 0.28%, and the yield is 78.13%, with the sulfur content of middlings was 1.62%, 1.73% respectively, and the yield was 4.75% and 8.88%. In order to further improve the concentrate grade and recovery and achieve better sulfur removal effect, the middlings in

the subsequent closed-circuit process test of one roughing, one cleaning and one scavenging are returned to the roughing process.
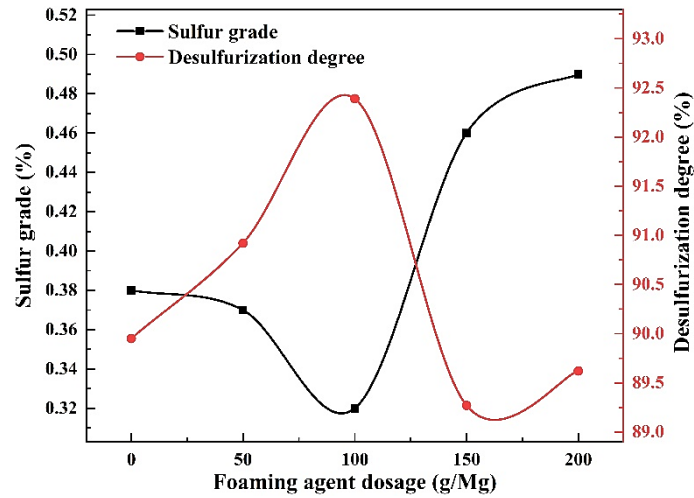

Fig. 8. Effects of foaming agent dosage on desulfurization

3.1.2. Laboratory closed-circuit experiment

Under the optimized conditions, one roughing, one cleaning as well as one scavenging flotation were carried out according to the flowsheet presented in Fig. 9. Table 4 presents the data provided by the experiments. The concentrate with the Al_2O_3 content of 68.28% and the recovery of 92.96% were achieved. In addition, the grade of sulfur was lowered to 0.33%, and the desulfurization efficiency reached up to 89.41%, which indicates that PYDH has a good desulfurization effect on high-sulfur bauxite，and could be used as an efficient collector of pyrite in the reverse flotation of high-sulfur bauxite.
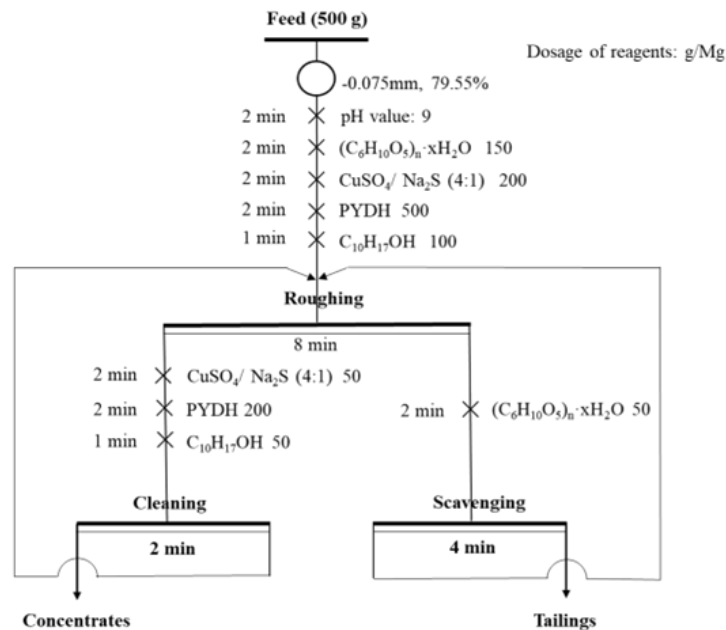

Fig. 9. Flowsheet of closed-circuit flotation

Table 4. Results of closed-circuit flotation

Products	Yield/wt %	$\omega(Al_2O_3)/\%$	$\varepsilon(Al_2O_3)/\%$	$\omega(S)/\%$	$\varepsilon(S)/\%$
Concentrate	90.16	68.28	92.96	0.33	10.59
Tailings	9.84	47.40	7.04	25.54	89.41
Feed	100.00	60.97	100.00	3.35	100.00

3.2.   Surface interaction of pyrite with the mixed collector

3.2.1. SEM–EDS studies

The results of SEM images and EDS spectra of pyrite observed in the presence and absence of PYDH are shown in Figure 10. Figures 10 (a) and (c) indicate that the surface of pyrite particles is relatively smooth, with some small particles on the surface, which may be due to partial oxidation of pyrite (Yin et al, 2018). In addition, the surface of pyrite becomes rough after interacting with PYDH and is covered by a large number of fine particles, as shown in Figure 10 (b) and (d). Table 5 summarizes the data obtained from the EDS spectra of pyrite before and after adsorption of mixed collectors, with each data point being measurements of 9 points on a sample for averaging. As shown in Table 5, there is a significant increase in the surface C mass ratio of pyrite, further verifying the adsorption of PYDH on pyrite.

Table 5. EDS spectra of pyrite and pyrite with PYDH

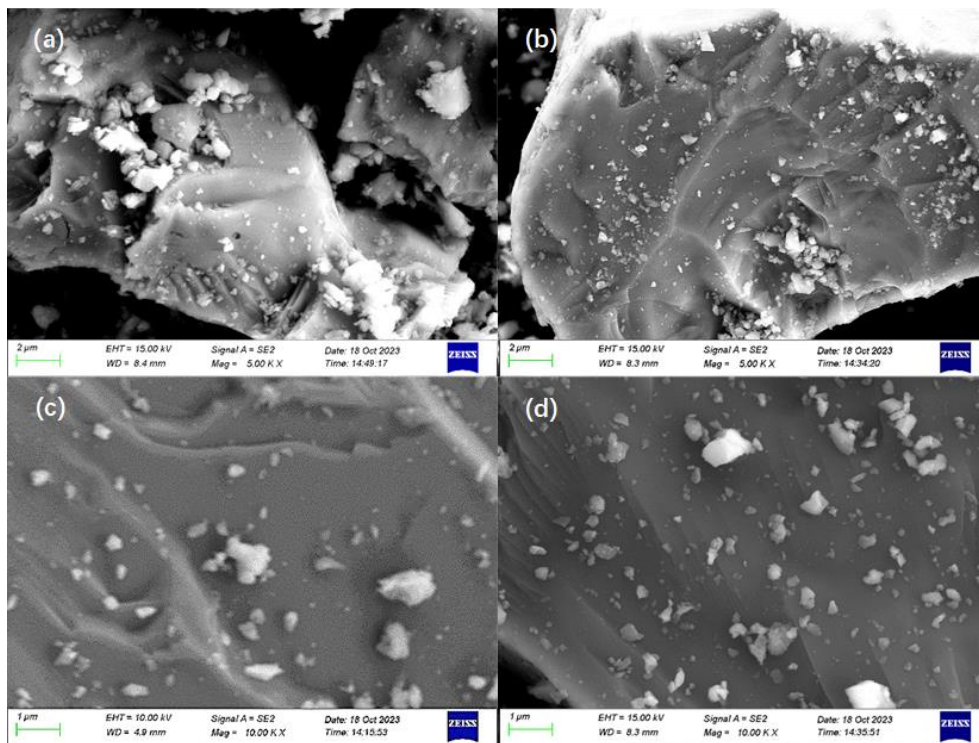| Pyrite		Pyrite with PYDH	
Element	Weight%	Element	Weight%
C	14.46	C	18.31
O	3.30	O	3.70
Fe	40.70	Fe	38.71
S	41.03	S	38.84

Fig. 10. SEM images of (a, c) pyrite and (b, d) pyrite with PYDH

3.2.2. Contact angle measurement

In order to compare the effects of adding mixed collectors and collectors alone on the floatability of pyrite, contact angle tests were conducted. Table 6 summarizes the data on the changes in surface contact angle of pyrite. From the data in Table 6, it can be seen that the contact angle on the surface of pyrite significantly increases when combined with HX, HD, and PYDH. Among them, the contact angle on the surface of pyrite after interaction with PYDH is the highest, at 99.0 °, indicating that the mixed

collector can better improve the hydrophobicity of the pyrite surface than the single collector, which is conducive to the flotation of pyrite.

Table 6. Contact angles of pyrite before and after interacting with collectors

Collectors	none	HX	HD	PYDH
Contact angles/°	35.4	93.3	94.2	99.0

3.3. Interaction mechanisms of the mixed collector with pyrite

3.3.1. Zeta potential analysis

The main results obtained from Zeta potentials of pyrite before and after interacting with collectors are summarized in Fig. 11. This figure shows that under the test pH (4-10), the Zeta potential of pyrite is all negative. Before interacting with the collector, the negative Zeta potential of pyrite has increased with the increase of solution pH. In the presence of HX and HD alone, the Zeta potential of pyrite significantly decreases, indicating strong adsorption of HX anions and HD anions on the surface of pyrite. Similarly, in the presence of PYDH, the Zeta potential of pyrite also significantly decreases. In addition, the Zeta potential shift of pyrite in the presence of HX is smaller than that of HD, and the Zeta potential of the PYDH etween HX and HD. The results indicate that HX, HD, and PYDH can all generate chemical adsorption on the surface of pyrite.
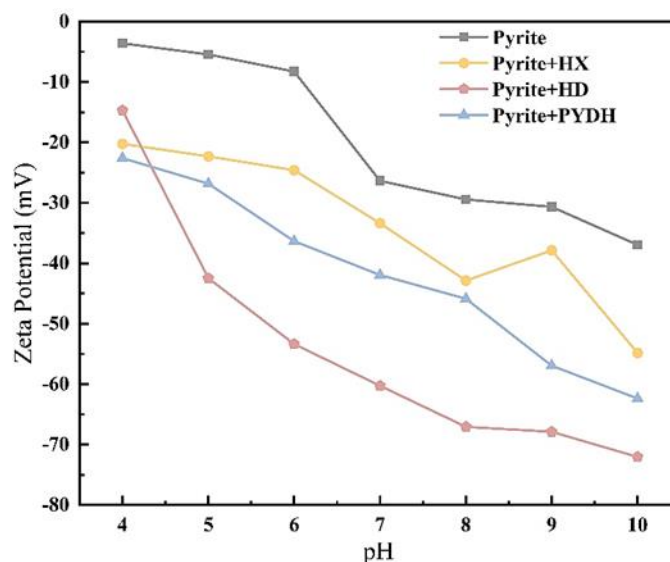

Fig. 11. Zeta potentials of pyrite in the presence of various collectors

3.3.2. FTIR-spectra analysis

In order to further verify the interaction mechanisms of PYDH with pyrite, FTIR analysis of the pyrite was conducted. Fig. 12 shows the data on FTIR results of pyrite before and after adsorbing different collectors. Before interacting with collector, 2937, 1082, 627 cm^{-1} were the characteristic peaks of pyrite, corresponding to the vibration peaks of Fe-OH, Fe-S and Fe-O, respectively (Chai et al, 2018; Sun et al, 2021). The intense and broad band centred at 3394 cm^{-1} and the peak at 1632 cm^{-1} are attributed to -OH in water (Oliveira et al, 2016). After interacting with HX, an additional new peak at 1030 cm^{-1} appeared in the spectrum, which resulted from the stretching vibration of C-O-C in HX. It proved that HX was adsorbed on pyrite surfaces. Meanwhile, C=S and C-S stretching vibration absorption peaks appear at 1192 cm^{-1} and 1171 cm^{-1}. In addition, the original peaks at 1082 cm^{-1} and 627 cm^{-1} are caused by Fe-S and Fe-O, shifted to 1096 cm^{-1} and 623 cm^{-1}, which indicates that HX is adsorbed on the pyrite surface by the chemical interaction of the Fe atom site. This is consistent with the research findings of other scholars (Zhang et al, 2013). After interacting with HD, two new peaks at 1018 cm^{-1} and 974 cm^{-1} appears in the spectrum, corresponding to the stretching vibration of C-O and P-O in HD, indicating

that HD was also adsorbed on pyrite surface. Closer observation of the figure shows that the new peak at 836 cm^{-1} could be attributed to the stretching vibration of P=S. In addition, the original peaks at 1082 cm^{-1} and 627 cm^{-1} caused by Fe-S and Fe-O, shifted to 1092 and 625 cm^{-1}, confirming that HD is also adsorbed on the pyrite surface by the chemical interaction of the Fe atom site likewise. After interacting with mixed collector, the original peaks at 1082 cm^{-1} and 627 cm^{-1}, because of stretching vibration of Fe-S and Fe-O, shifted to 1100 cm^{-1} and 628 cm^{-1}. Except for the characteristic peaks of HX and HD themselves, no new peaks were found, indicating that there was no chemical bond breakage and reorganization between the mixed collector PYDH, but rather that each showed chemical interaction on pyrite. These findings are consistent with zeta potential results.
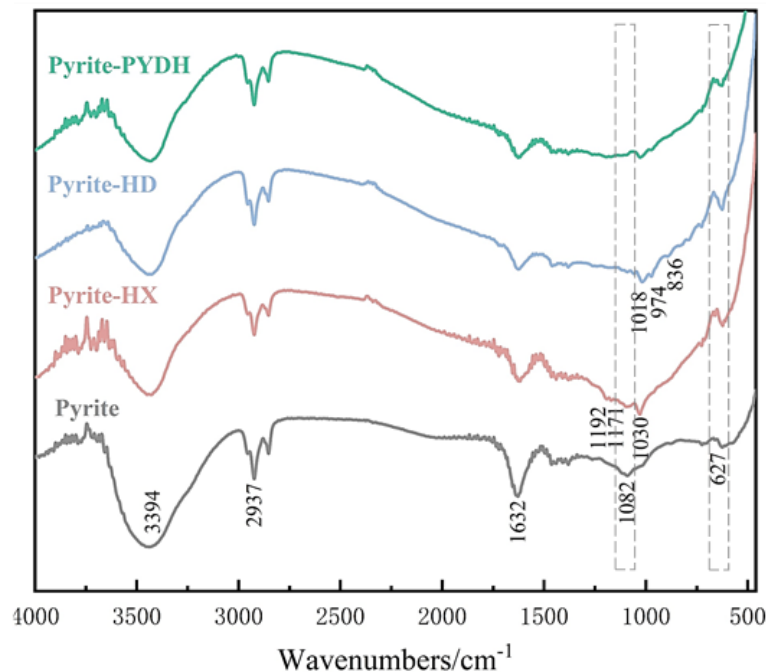

Fig. 12. FTIR spectra of pyrite in the presence of various collectors

3.3.3. XPS investigation

XPS was used to characterize the elemental compositions and chemical states of the pyrite surface with and without PYDH. Fig. 13 (a) and (b) details the data on the XPS of Fe 2p and S 2p before and after interacting with PYDH, and Table 7 demonstrates the XPS binding energies. The Fe $2p_{1/2}$ and Fe $2p_{3/2}$ XPS bands of pyrite are observed at 719.2 and 706.4 eV (Moulder et al, 1992). Besides, at 710.6 eV, it belongs to Fe-O species, indicating partial oxidation on the surface of pyrite, which is consistent with the FTIR-spectra analysis results. There is a clear difference between XPS spectrum of pyrite and pyrite-PYDH. After interacting with PYDH, the Fe $2p_{1/2}$ signal weakened and shifted slightly from 719.2 to 718.4 eV, the XPS band of the Fe-S species decreased by 0.3 to 706.1 eV, and the XPS band of the Fe-O species shifted to a lower binding energy (710.1 eV). These results indicate that the PYDH molecules react chemically with Fe atoms on the surface of pyrite, and new Fe-S as well as Fe-O bonds were generated. In the meantime, the pyrite S $2p_{1/2}$ and S $2p_{3/2}$ XPS band was located at 162.9 and 161.8 eV (Moulder et al, 1992), after interacting with PYDH, the peaks become weaker and shifted to 162.7 and 161.5 eV. These changes further demonstrate the chemical adsorption of PYDH on the pyrite surface and the formation of Fe-S bonds.

Table 7. Binding energies of pyrite before and after interacting with PYDH

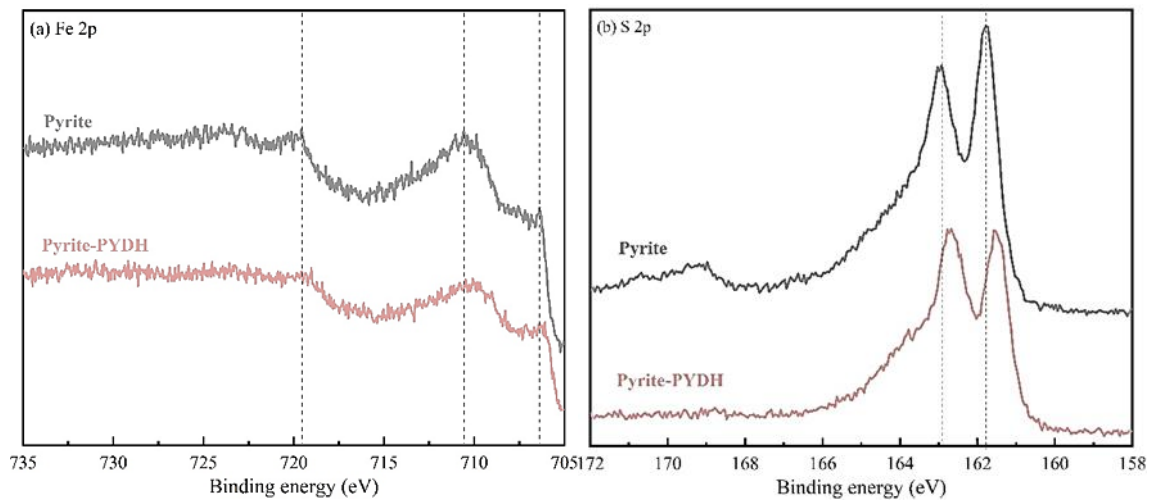| Samples	Binding energy/eV	
	Fe 2p	S 2p
Pyrite	719.2, 710.6, 706.4	162.9, 161.8
Pyrite-PYDH	718.4, 710.1, 706.1	162.7, 161.5

Fig. 13. High-resolution Fe 2p XPS (a) and S 2p XPS (b) spectra of pyrite and pyrite with PYDH

4. Conclusions

This study determined the optimal process conditions for flotation desulfurization of high sulfur bauxite as follows: grinding fineness of -0.075mm, 79.55%, pulp pH of 9, inhibitor of 150 g/Mg, activator of 200 g/Mg, collector of 500 g/Mg, and foaming agent of 100 g/Mg. Better flotation results were achieved. After a closed-circuit flotation process of one roughing, one cleaning, and one scavenging, the alumina content in the concentrate is 68.28%, the sulfur content is 0.33%, the alumina recovery rate is 92.96%, and the desulfurization rate reaches 89.41%. The flotation desulfurization test effect of the mixed collector PYDH is better than that of HX or HD.

On the other hand, research on the interaction mechanism between mixed collectors and pyrite shows that PYDH adsorbed on the surface of pyrite and weaken the negative Zeta potential of pyrite. In addition, compared to using HX or HD alone, the mixed collector PYDH can better improve the hydrophobicity of pyrite surface. Further analysis indicates that PYDH is chemically adsorbed on the surface of pyrite by combining - S in the collector with Fe atoms on the pyrite to form Fe-S.

Acknowledgments

References

ABIKENOVA G.K., KOVZALENKO V.A., AMBARNIKOVA G.A., ET AL. 2008. *Investigation of the effect and behavior of sulfur compounds on the technological cycle of alumina production*. Russ. J. Non-ferrous Metals. 49, 91-96.

AWE A.A., SUNDKVIST J.E., SANDSTRÖM Å., 2013. *Formation of sulphur oxyanions and their influence on antimony electrowinning from sulphide electrolytes*. Minerals Engineering. 53, 39–47.

BARBOSA F.M., BERGERMAN M.G., HORTA D.G., ET AL. 2016. *Removal of iron-bearing minerals from gibbsitic bauxite by direct froth flotation, Technol*. Tecnologia em Metalurgia, Materiais e Mineração. 13(1), 106-112.

BLIGHT K., RALPU D.E., THURGATE S. 2000. *Pyrite surfaces after bio-leaching: a mechanism for bio-oxidation*. Hydrometallurgy. 58(3), 227-237.

BULUT G., ARSLAN F., ATAK S., ET AL. 2004. *Flotation behaviors of pyrites with different chemical compositions*. Mining, Metallurgy & Exploration. 21, 86-92.

CALDEIRA C.L., CIMINELLI V.S.T., DIAS A., ET AL. 2003. *Pyrite oxidation in alkaline solutions: Nature of the product layer* [J]. International Journal of Mineral Processing. 72(1-4), 373-386.

CHAI W.C., HUANG Y.F., PENG W.J., ET AL. 2018. *Enhanced separation of pyrite from high-sulfur bauxite using 2-mercaptobenzimidazole as chelate collector: Flotation optimization and interaction mechanisms*. Minerals Engineering. 129, 93-101.

ERSOY Ö.F., TURGUT H., Güven O., ET AL, 2013. *Effect of heat treatment on the flotation of Turkish lignites in brine solution*. Materials Science and Technology. 10, 2044-2052.

GE L., GONG X.Z., 2015. *Sulfur removal from bauxite water slurry (BWS) electrolysis intensified by ultrasonic*. Ultrasonics Sonochemistry, 26, 142–148.

GIBSON B., WONYEN D.G., CHELGANI S.C. 2017. *A review of pretreatment of diasporic bauxite ores by flotation separation* [J]. Minerals Engineering. 114, 64-73.

HE M.F., LI S.K., CAO M., ET AL. 2021. *Activation mechanism of tantalum niobium flotation by lead ions in a combined collector flotation system*. Physicochemical Problems of Mineral Processing. 57(1), 29–38.

LI M.X., CHEN X.H., WANG S., et al. 2015. *Study on the desulfurization mechanism of high-sulfur bauxite by microwave*. Light Metals. 01, 16–19.

LIU H., HE J., LUO T., ET AL. 2023. *Interfacial Adsorption Mechanism of Diethyldithiocarbamate in High-Sulfur Residue Flotation*. Processes. 11(5), 1568.

LIU Z., YAN H., MA W., ET AL. 2020. *Digestion behavior and removal of sulfur in high-sulfur bauxite during bayer process*. Minerals Engineering, 149(2), 106237.

LOU Z., XIONG Y., FENG X., ET AL. 2016. *Study on the roasting and leaching behavior of high-sulfur bauxite using ammonium bisulfate* [J]. Hydrometallurgy. 165, 306–311.

MONDILLO N., HERRINGTON R., BONI M. 2021. *Encyclopedia of Geology*. Academic Press. 5, 694-707.

MOULDER J.F., CHASTAIN J., KING R.C., ET AL. 1992. *Handbook of x-ray photoelectron spectroscopy: a reference book of standard spectra for identification and interpretation of XPS data*. Chemical Physics Letters. 220(1), 7-10.

OLIVEIRA C.M., MACHADO C.M., DUARTE G.W., ET AL. 2016. *Beneficiation of pyrite from coal mining*. Journal of Cleaner Production. 139, 821-827.

PARASKEVAS D., VOORDE A.V.D., KELLENS K., ET AL. 2016. *Current Status, Future Expectations and Mitigation Potential Scenarios for China's Primary Aluminium Industry*, Procedia CIRP, 295-300.

SUN Q., WANG S., MA X., ET AL. 2021. *Desulfurization in high-sulfur bauxite with a novel thioether-containing hydroxamic acid: Flotation behavior and separation mechanism*. Separation and Purification Technology. 275, 119147.

TABEREAUX A.T., PETERSON R.D. 2014. *Aluminum Production*. Treatise on Process Metallurgy. 3, 839-917.

TAGUTA J., O'CONNOR C.T., MCFADZEAN B., ET AL. 2003. *The effect of the alkyl chain length and ligand type of thiol collectors on the heat of adsorption and floatability of sulphide minerals*. Minerals Engineering. 110, 145-152.

VEAR M., SCHIPPERS A., SAND W., ET AL. 2013. *Progress in bioleaching: fundamentals and mechanisms of bacterial metal sulfide oxidation – part A*. Applied Microbiology & Biotechnology. 97(17), 7529-7541.

XIE W.K., ZHOU Z.Q., CHEN X.H., 2017. *Study on the Flotation Desulfurization of High-sulfur Bauxite in Henan*[J]. Nonferrous Metals (Mineral Processing Section). 01, 43-45.

YANG X.L., ALBIJANIC B., LIU G.Y., ET AL. 2018. *Structure–activity relationship of xanthates with different hydrophobic groups in the flotation of pyrite*. Minerals Engineering. 125, 155–164.

YIN W.Z., XUE J.W., LI D., ET AL. 2018. *Flotation of heavily oxidized pyrite in the presence of fine digenite particles*. Minerals Engineering. 115, 142-149.

YU, S.X., SUN, W., WANG, Y.L., ZHANG, P., 2002. *Recycling uses of wastewater from flotation of phosphate ores by electrochemical treatment*. Industrial Water Treatment. 22(2), 12-14.

ZHANG Y.H., CAO Z., CAO Y.D., ET AL. 2013. *FTIR studies of xanthate adsorption on chalcopyrite, pentlandite and pyrite surfaces*. Journal of Molecular Structure. 1048, 434-440.

ZHANG N., ZHOU C., CONG L., ET AL. 2016. *Semi-industrial experimental study on bauxite separation using a cell-column integration process*. Int. J. Miner. Metallurgy Mater. 23, 7–15.

ZHOU J., MEI G., YU M., ET AL. 2019. *Effect and mechanism of surface pretreatment on desulfurization and desilication from low-grade high-sulfur bauxite using flotation*. Physicochemical Problems of Mineral Processing, 55(4): 940-950.

ZHOU J.Q., MEI G.J., YU M.M., ET AL. 2022. *Effect and mechanism of quaternary ammonium salt ionic liquid as a collector on desulfurization and desilication from artificial mixed bauxite using flotation*. Minerals Engineering. 181, 107523.

ZHU Z.P., TENG X., YANG Y., ET AL. 2023. *Flotation Decarbonization and Desulfurization of a High-Sulfur Bauxite in China*. Minerals. 13(8), 1008.